TIME-TO-DEPTH MAPPING AND IMAGING OF TIME-MIGRATED SEISMIC DATA WITH INHERENT VELOCITY ESTIMATION

E. Iversen and M. Tygel

email: *einar.iversen@norsar.com*

keywords: *Image ray, time-to-depth conversion, time migration*

ABSTRACT

For cases where time migration yields well-focused images, we introduce a procedure for mapping and imaging, respectively, selected events and complete time-migrated data to the depth domain. A basic assumption is the existence of an appropriate field of time-migration velocities. We utilize the image-ray concept, invented by Hubral in 1977, for the transformation of events or seismograms from the time-migrated domain to the depth domain. The calculation of image rays relies on the knowledge of ray velocities while the available input velocities in this context are given in the form of a time-migration velocity field. The required ray velocities are obtained from the given migration velocity field by means of the classical Dix algorithm and elements of the ray propagator matrix, i.e., paraxial ray-tracing matrices corresponding to a plane wavefront and a point source in the starting point of the image ray. The numerical integration is formulated as an independent process for each image ray and makes use of ordinary differential equations for the position/slowness vectors (kinematic ray-tracing equations) and the ray propagator matrix expressed in ray-centered coordinates (dynamic ray-tracing equations). Integration of the ray differential equations provides a field of image-ray points and corresponding ray velocities belonging to the depth domain. For each available image ray, one can image an entire seismic trace or map a number of selected events from the time-migrated domain to the depth domain. A final step of the proposed time-to-depth conversion procedure is to perform regularization of the estimated ray-velocity field, mapped seismic events, and imaged seismic data with respect to the depth-domain coordinates.

INTRODUCTION

Time migration is a well-established and routinely applied procedure to obtain time-domain images from seismic reflection data. The main advantages of the time-migration procedure is that it is fast, inexpensive and, except for strong lateral velocity variations, very robust with respect to inaccuracies of the time-domain velocity model. This is to be compared with the much more involved depth migration, especially prestack, which requires, besides a well designed depth-domain velocity model, also significantly more computational effort.

As compared to common-midpoint (CMP) stacking, which essentially produces sections of seismic data corresponding to a simulated zero offset (ZO) acquisition, the time migration process generates sections with features that are more easily identified with structures in the depth domain. In particular, triplications typical for unmigrated images of synclinal structures naturally unfold to synclinals after time migration.

For any time-domain imaging procedure, the image of a reflector is called a "reflecting horizon". For the same reflector in the depth domain, the overall characteristics, kinematic and dynamic, of its corresponding reflecting horizon will be strongly dependent on the acquisition configuration and imaging procedure that is employed.

In accordance to the ray-theoretical methods that will be used throughout, we envisage the reflector as a continuum of independent point scatterers (or point diffractors), which, due to seismic illumination, are excited and emit energy towards the surface. Under this formulation, the image of a reflector can be understood as the ensemble of the individual (time-domain) images of the point scatterers that constitute the (depth-domain) reflector.

The basic goal of time migration is to focus the seismic energy into interpretable images in the time domain of the seismic data. In this respect, time migration has a very useful property, as opposed to depth migration, in that a well-focused image can often be obtained even for a very simple velocity model. Moreover, this focusing property of the time-migration process is quite robust with respect to perturbations of the time-migration velocity model. However, since time migration is commonly based on a hyperbolic traveltime approximation, its applicability is limited to velocity models with slow lateral variations (Yilmaz, 2000). Historically speaking, "ideal" or "complete" time migration has been considered as a process positioning the reflecting horizons "vertically above" their corresponding depth-domain reflectors. More specifically, the horizontal coordinates of each point scatterer on a reflector would then coincide with the horizontal coordinates (trace location) of its associated time-migrated image. For this idealized process, it is assumed that the connection between each point scatterer at the reflector and its trace location at the surface can be realized by a vertical ray. As a consequence, the transformation of the traveltime coordinate of a point on a time-migrated reflecting horizon and the depth coordinate of its associated point scatterer at the reflector (the so-called time-to-depth conversion) would be achieved by a simple scaling operation, namely, the multiplication of half the traveltime by an appropriate (average) medium velocity along the vertical ray.

The above concept of a complete time migration, although useful as a theoretical framework, is not possible to be realized. As explained in Hubral (1977) , the closest feasible alternative is to have a transformation that uses *image rays* (and not vertical rays) to connect the point scatterers at the reflector to their corresponding trace locations at the surface. For an arbitrary point scatterer on the depth-domain reflector, the *image ray* can be defined as a ray connecting the scatterer to the measurement surface in such a way that the slowness vector is normal to that surface. This definition allows the medium below the measurement surface to be either isotropic or anisotropic. Likewise, the *normal ray* can be defined as a ray connecting the point scatterer to the measurement surface in such a way that the slowness vector is normal to the depth-domain reflector (Iversen, 2006). As also described in Hubral (1977), assuming an isotropic velocity model, the following analogy exists between normal rays and image rays that connect the surface measurement to a given reflector scatterer: the former is normal to the reflector, whereas the latter is normal to the measurement surface.

Kirchhoff depth migration: A good understanding on how time migration can be actually realized can be gained by examining its relationship to Kirchhoff depth migration, as applied to a single stacked section. Such a procedure is referred to as 2D Kirchhoff poststack depth migration. For a given depth-domain macro-velocity model and also a given point in the depth domain, M, to be imaged, the Kirchhoff depth migration operation basically consists of a weighted sum of data samples along the diffraction time surface associated to M, the result of that sum being assigned at M. Under the assumption that a stacked section well approximates (or simulates) a ZO section, the diffraction time surface associated to the fixed point M is given by the two-way times along the rays that connect M to the varying coincident (ZO) source-receiver points at the measurement surface. According to the theory of Kirchhoff migration (see, e.g., Tygel et al., 1996), for a sufficiently accurate macro-velocity model, the summing operation along the diffraction time surface that is associated to a point at a reflector will be (approximately) tangent to its corresponding reflecting horizon in the stacked section. As a consequence, the Kirchhoff summation will provide significant values at the image points, M, which lie at (or are very close to) a reflector. For image points, M, away from the reflectors, the corresponding summation values will find negligible values. The migrated depth-domain section is obtained by applying the above described Kirchhoff summation to a previously defined dense grid of image points, M.

The above considerations show that the Kirchhoff process realizes, for any individual depth reflector, a correspondence (or mapping) between each point scatterer on the reflector and the tangency point where the diffraction traveltime surface associated with the point scatterer meets the reflecting horizon in the

stacked section. Hubral (1977) refers to these tangency points as “scattering centers for seismic waves". The Kirchhoff migration associates, thus, each scatterer on the reflector to its corresponding scattering center at the reflecting horizon. We finally observe that any point scatterer on the reflector is connected to the projection on the measurement surface of its corresponding scattering center by the normal ray.

For an isotropic depth velocity model with no lateral variations and horizontal interfaces, it is clear that, for each point scatterer on a reflector, the normal and image rays coincide, being both vertical. In this case, the stacked section also coincides with the time-migrated section, and that also represents a “complete" time migration, which corresponds to vertical image rays. Apart from this extremely simple situation, we have that stacking and time migration are bound to yield very different images of the same depth model.

Kirchhoff time migration: Time migration can be realized by a simple modification to the above described Kirchhoff poststack depth migration. After stacking along the diffraction traveltime surface of a given depth point, M, all we need to do is to assign the stacking result (the migration output) at the *apex of the diffraction traveltime source*, instead of assigning it to the original depth point M, as would be done in the Kirchhoff depth migration counterpart. The reasoning for the above approach is simple: the apex of the diffraction traveltime surface from a point scatterer M represents the least traveltime from that point to the measurement surface. As a consequence, the image ray from M is the one that realizes that minimum traveltime.

An underlying assumption of the procedure is that the diffraction traveltime surface is sufficiently well behaved, so that a clear apex exists. In the absence of abrupt lateral velocity variations, each diffraction traveltime surface can be well approximated by a hyperboloid in the vicinity of its apex. Based on the above considerations, it is now possible to formulate a time migration procedure that is based on time-domain computations only, so that the dependency on a depth-domain macro-velocity can be avoided. As well known in the literature (see, e.g., Hubral and Krey, 1980), one way to do it is to apply on the stacked seismic data a so-called migration velocity analysis and stacking procedure. Consider for simplicity a single (say, post stack), time-migrated section where the in-line coordinate is the scalar x^M and the two-way time is denoted as t^M. For each given point (x^M, t^M) in the time-migrated section to be constructed, we consider the hyperbolic traveltime

$$t^2 = (t^M)^2 + \frac{4}{(\mathcal{V}^M)^2}(x - x^M)^2 \tag{1}$$

defined for each trial migration velocity, $\mathcal{V}^M$, and along which samples, (x, t), in the given post stack (ZO) section are stacked. If the point (x^M, t^M) actually belongs to a time-migrated reflecting horizon, a migration velocity, $\mathcal{V}^M$ would exist such that the time $t(x)$ in equation (1) would well approximate a diffraction traveltime function for a certain point scatterer on a depth reflector. As such, the traveltime function $t(x)$ in equation (1) would be tangent to the reflecting horizon in the stacked section that relates to that depth-domain reflector. Based on the above considerations, coherence analysis may be applied to determine the migration velocity $\mathcal{V}^M$ associated to a point (x^M, t^M) in the time-migrated section. Note that the described migration-velocity analysis is much related to its counterpart common-midpoint (CMP) velocity analysis designed to obtain the normal-moveout (NMO) velocity field and its corresponding stacked (ZO) section.

As a result of migration-velocity analysis and stacking applied to the unmigrated section, one obtains, besides a time-migrated section, also a migration velocity field. An in-depth description of the various methods to perform Kirchhoff time migration and migration-velocity analysis is away from the scope of the present paper. For that, the reader is referred to, e.g., Yilmaz (2000) and the references therein. Here we only briefly indicate how the migration velocity can be obtained: one option frequently used in the past was to use the stacking (NMO) velocity that has previously been determined for obtaining the CMP-stacked stacked section and eventually apply an ad hoc scaling factor to it. For dipping structures, an approach often considered as more adequate is to use as migration velocity an NMO velocity that has been properly corrected for dip-moveout (DMO), see Hale (1984). Finally, as an example of a modern, automated, migration-velocity estimation approach, we refer the reader to Fomel (2003).

Time-do-depth conversion: The final aim of (kinematic) seismic imaging is to position reflectors correctly in the depth domain. In this way, time-domain images such as CMP-stacked or time-migrated

sections represent intermediate, although very useful, results. A subsequent operation that transforms a time-domain seismic data set into its corresponding depth-domain data set is referred to as *time-to-depth migration* or *time-to-depth conversion*. The terminology *time-to-depth mapping* is also employed when only selected time-domain horizons are migrated into the depth domain.

Assume, for simplicity, that the measurement surface is a horizontal plane, located at zero depth. Moreover, let the unmigrated data set be described by the coordinates (x_1^U, x_2^U, t^U), where the first two coordinates, x_1^U and x_2^U, specify the location of the CMP on the measurement surface and the third coordinate, t^U, is time. The superscript U signifies that the coordinates belong to the "unmigrated time domain". Time-to-depth conversion of an unmigrated data set requires that normal rays can be traced from the measurement surface. This is possible if information from the the time-domain data set, as well as adequate structural assumptions for the subsurface, allows one to derive a suitable depth-domain velocity model and, in addition, the initial directions of the normal rays. In this situation, time-to-depth conversion means to move the event located at the point (x_1^U, x_2^U, t^U) along a normal ray that starts at the CMP and proceeds to its endpoint, determined by the criterion that half of the given time, $t^U/2$, is consumed.

Under the assumption of a 3D iso-velocity layered model with smoothly curved interfaces, Hubral and Krey (1980) proposed a recursive algorithm to recover the layer velocities, as well as the positions and curvatures of the interfaces, from the knowledge of the traveltime function and the first two derivatives with respect to the coincident source-receiver horizontal location of each reflecting horizon in the unmigrated data set. Geometrically, the first derivative of traveltime is related to the angle of incidence of the normal ray. The second derivative is related to the radius of curvature of the so-called NIP wave at the emergence point of the normal ray.

In an analogous manner to the previous considerations, time-to-depth conversion of time-migrated seismic data will be possible if the information in the time-domain data allows one to trace image rays in the depth domain. An advantage of such a process, as compared to the previous case involving the unmigrated data set, is that image rays have a known initial condition, namely, that the initial slowness vector is perpendicular to the measurement surface. For each point (x_1^M, x_2^M, t^M) in the time-migrated domain, the time-to-depth conversion moves the event at this point along the image ray that starts at $(x_1 = x_1^M, x_2 = x_2^M, x_3 = 0)$ on the measurement surface and proceeds into the depth domain until half of the given time, $T = t^M/2$, is consumed. For a 3D iso-velocity layered macro-velocity model in the depth domain, Hubral and Krey (1980) described an algorithm to transform along image rays the locations, dips, and curvatures for horizon points in the time-migrated domain to corresponding locations, dips, and curvatures for horizon points in the depth domain. A generalization of this algorithm to include heterogeneous layers was described by Iversen et al. (1987) and Iversen et al. (1988).

In this paper we present a method to convert a given time-migrated section, for which the time-migration velocity is known, into its corresponding depth section. The procedure uses image rays that are traced into depth using solely the time-migration velocities. Our approach has much in common with the very recent works of Filpo and Portugal (2006) and Cameron et al. (2006), however with significant differences. The presented approach can better accommodate lateral velocity variations than in Filpo and Portugal (2006) and also uses a full 3D formulation, as opposed to the 2D approach presented in Cameron et al. (2006).

NOMENCLATURE

In order to facilitate following the mathematical derivations and also the appreciation of the obtained results, we list below the notation that is used throughout. Lower and upper case letters, i and I, used as subscripts may have the values $i = 1, 2, 3$, and $I = 1, 2$, respectively. For three-component vectors we use standard notation, e.g., $\mathbf{a}$, while for two-component vectors a bar is written above the symbol, e.g., $\bar{\mathbf{a}}$. Vectors are equivalently considered as column matrices. To distinguish between matrices of size 3×3 and 2×2, we use the notations $\hat{\mathbf{A}}$ and $\mathbf{A}$, respectively. The notation $\mathbf{A}^T$ is used for the transpose of the matrix $\mathbf{A}$, while $\mathbf{A}^{-T}$ is a shorthand notation for $\mathbf{A}^{-1^T}$. In cases where ambiguity may arise, a superscript in the form (q) on vectors/matrices serves as a label for the coordinate system under consideration. The 3×3 matrix containing the second-order partial derivatives of a scalar field V is written in the form

$$\frac{\partial^2 V}{\partial \mathbf{x}^2} = \left(\frac{\partial^2 V}{\partial x_i \partial x_j} \right) . \tag{2}$$

Symbol	Meaning
$\mathbf{x} = (x_1, x_2, x_3 = z)$	Point in depth-domain Cartesian coordinates
$\boldsymbol{\gamma}^M = (x_1^M, x_2^M, x_3^M = t^M)$	Point in time-migration domain Cartesian coordinates
$\boldsymbol{\gamma} = (\gamma_1^M = x_1^M, \gamma_2^M = x_2^M, T = t^M/2)$	Ray coordinates to specify a point along the image ray
$V(\mathbf{x})$	Depth-domain velocity field
$\mathcal{V}^M(\boldsymbol{\gamma}^M)$	Time-migration velocity field
$\mathcal{V}_{dix}^M(\boldsymbol{\gamma})$	Time-migration interval velocity field
$\mathcal{V}(\boldsymbol{\gamma})$	Ray velocity along the image ray
$F(\boldsymbol{\gamma})$	Migration velocity spreading factor
$\mathbf{x}(\boldsymbol{\gamma}), \mathbf{p}(\boldsymbol{\gamma})$	Position and slowness vectors along the image ray
$\hat{\mathbf{Q}}^{(x)}(\boldsymbol{\gamma})$	First paraxial 3×3 matrix, in depth-domain Cartesian coordinates
$\hat{\mathbf{Q}}^{(q)}(\boldsymbol{\gamma})$	Ray-centered first paraxial 3×3 matrix along the image ray
$\mathbf{Q}_I^{(q)}(\boldsymbol{\gamma}), \mathbf{P}_I^{(q)}(\boldsymbol{\gamma})$	Ray-centered first and second paraxial 2×2 matrices along the image ray
Q_1	The "11" element of matrix $\mathbf{Q}_1^{(q)}$
P_1	The "11" element of matrix $\mathbf{P}_1^{(q)}$
Q_2	The "11" element of matrix $\mathbf{Q}_2^{(q)}$
P_2	The "11" element of matrix $\mathbf{P}_2^{(q)}$

THEORY

To describe the time-to-depth conversion algorithm that is proposed here, we start by specifying the input data that is needed to initialize the process.

Input data: As input to the combined velocity estimation and time-to-depth-conversion procedure, we assume the knowledge of a migration-velocity function for one particular seismic profile direction, $\mathcal{V}^M = \mathcal{V}^M(x_1^M, x_2^M, t^M)$, where (x_1^M, x_2^M) are horizontal coordinates within the datum plane, i.e., coordinates specifying a trace in the time-migrated data set, and t^M denotes the (two-way) migration time. Values of the migration-velocity function shall be available on a regular grid in the time-migration domain coordinates x_1^M, x_2^M, and t^M. In the following, we also introduce the *ray-domain coordinate vector*, $\boldsymbol{\gamma} = (x_1^M, x_2^M, T = t^M/2)^T$, with the understanding that the time-migrated domain is a natural ray domain for image rays. Each image ray, $\mathbf{x} = \mathbf{x}(\boldsymbol{\gamma})$, is specified by setting the first two ray parameters, x_1^M and x_2^M, constant and having T as a variable along the ray. The velocity along the image ray will be denoted as $\mathcal{V} = \mathcal{V}(\boldsymbol{\gamma})$ and referred to as the *ray velocity*.

Ray velocities as a function of ray-domain coordinates: Our first task in the time-to-depth conversion method that is presented here is to find the relationship between the given time-migration velocities and the velocities that will be assigned to the image rays as they are traced into depth. In other words, we need to convert the given time-migration velocity field to a corresponding image-ray velocity field in depth. At first, the image-ray velocity field will be given in the image-ray coordinates, $\mathcal{V}(\boldsymbol{\gamma})$. As a next stage, that velocity field will be transformed into a velocity field in depth-domain Cartesian coordinates, $V(\mathbf{x})$, in a natural way.

To accomplish this task, we follow Cameron et al. (2006) and recognize that the required relationship for a 2D procedure is based on the time-migration equation 1. For the 3D procedure described in this paper, equation 1 is still relevant, given that the distance, $x - x^M$, and the migration velocity, V^M, correspond to an arbitrary horizontal unit direction vector,

$$\bar{\mathbf{u}} = (\cos\theta, \sin\theta)^T, \tag{3}$$

specified by a profile angle, θ. Using the concepts and results of ray propagator matrices as provided in Hubral et al. (1992) and Iversen (2006), we show in Appendix A that

$$\mathcal{V}(\boldsymbol{\gamma}) = \mathcal{V}_{dix}^M(\boldsymbol{\gamma}) F(\boldsymbol{\gamma}), \tag{4}$$

where $\mathcal{V}_{dix}^M$ is the Dix velocity (time-migration interval velocity)

$$\mathcal{V}_{dix}^M(\boldsymbol{\gamma}) = \left\{ \frac{d}{dT^M}[T^M(\mathcal{V}^M)^2] \right\}^{1/2} = \left\{ \frac{d}{dT}[T(\mathcal{V}^M)^2] \right\}^{1/2}, \tag{5}$$

and F is the factor

$$F(\boldsymbol{\gamma}) = \frac{\bar{\mathbf{u}}^T \mathbf{I}^* \mathbf{Q}_1^{(q)^T} \mathbf{Q}_2^{(q)^{-T}} \mathbf{I}^* \bar{\mathbf{u}}}{\left\{ \bar{\mathbf{u}}^T \mathbf{I}^* \mathbf{Q}_2^{(q)^{-1}} \mathbf{Q}_2^{(q)^{-T}} \mathbf{I}^* \bar{\mathbf{u}} \right\}^{1/2}} \,. \tag{6}$$

In the above formula, $\mathbf{Q}_1^{(q)}$ and $\mathbf{Q}_2^{(q)}$ are the plane-wave and point-source first paraxial ray-tracing 2×2 matrices in the downward direction along the image ray, $\bar{\mathbf{u}}$ is the unitary profile direction vector given in equation 3, and $\mathbf{I}^*$ is the matrix

$$\mathbf{I}^* = \begin{pmatrix} -1 & 0 \\ 0 & 1 \end{pmatrix}. \tag{7}$$

In the 2D situation, the factor F reduces to the simple formula

$$F(\boldsymbol{\gamma}) = Q_1, \tag{8}$$

which is the one given in Cameron et al. (2006).

Relationships between ray- and depth-domain velocity fields: It is our aim to convert the ray-domain velocity field, $\mathcal{V}(\boldsymbol{\gamma})$, into a corresponding depth-domain velocity field, $V(\mathbf{x})$, in which the image rays will be traced. The relationship between the ray- and depth-domain velocity fields is defined by

$$V(\mathbf{x}) = V(\mathbf{x}(\boldsymbol{\gamma})) = \mathcal{V}(\boldsymbol{\gamma}). \tag{9}$$

Here, $\mathbf{x} = \mathbf{x}(\gamma)$ denotes the depth-domain trajectory of the image ray specified by the ray coordinates $\boldsymbol{\gamma}$.

For our purposes of tracing the image rays that will accomplish the proposed time-to-depth conversion procedure, we shall need, besides the relationship 9 between the ray- and depth-domain velocity fields, also the corresponding relationships between the first and second derivatives of these two velocity fields. The required relationships can be obtained by applying the chain rule of advanced calculus to equation 9 twice. The first application gives, in matrix form

$$\frac{\partial V}{\partial \mathbf{x}} = (\hat{\mathbf{Q}}^{(x)})^{-T} \frac{\partial \mathcal{V}}{\partial \boldsymbol{\gamma}} \,, \tag{10}$$

under the assumption that inverse matrix $(\hat{\mathbf{Q}}^{(x)})^{-1} = (\partial \gamma_i / \partial x_j)$ exists. We introduced the *first paraxial ray-tracing matrix* $\hat{\mathbf{Q}}^{(x)} = (\partial x_i / \partial \gamma_j)$ in depth-domain Cartesian coordinates and also the notations

$$\frac{\partial \mathcal{V}}{\partial \boldsymbol{\gamma}} = (\frac{\partial \mathcal{V}}{\partial \gamma_1}, \frac{\partial \mathcal{V}}{\partial \gamma_2}, \frac{\partial \mathcal{V}}{\partial \gamma_3})^T \quad \text{and} \quad \frac{\partial V}{\partial \mathbf{x}} = (\frac{\partial V}{\partial x_1}, \frac{\partial V}{\partial x_2}, \frac{\partial V}{\partial x_3})^T \,. \tag{11}$$

The existence of the inverse matrix $(\hat{\mathbf{Q}}^{(x)})^{-1}$ for all considered values of the ray coordinate vector $\boldsymbol{\gamma}$ ensures a one-to-one correspondence between ray- and depth-domain coordinates, $\mathbf{x} = \mathbf{x}(\boldsymbol{\gamma})$ and $\boldsymbol{\gamma} = \boldsymbol{\gamma}(\mathbf{x})$. This means, in particular, that each point in the depth domain can be connected to the measurement surface by at most one image ray only. This also means that the image-ray field cannot contain caustic points. As a final observation, the relationship between ray- and depth-domain velocity fields

$$\mathcal{V}(\boldsymbol{\gamma}) = \mathcal{V}(\boldsymbol{\gamma}(\mathbf{x})) = V(\mathbf{x}), \tag{12}$$

which is the inverse to the one given by equation 9, is also valid.

The 3x3 matrix $\hat{\mathbf{Q}}^{(x)}$ is one of two paraxial ray-tracing matrices with elements constituting the dependent variables of the dynamic ray-tracing system in Cartesian coordinates. The other one is the matrix $\hat{\mathbf{P}}^{(x)}$ with elements $P_{ij}^{(x)} = \partial p_i / \partial \gamma_j$, but this matrix is, however, not needed specifically in the following. To obtain the relationship between the second derivatives of the ray- and depth-domain velocities, we apply once more the chain rule, this time to equation 10. We get, also in matrix form

$$\frac{\partial^2 V}{\partial \mathbf{x}^2} = (\hat{\mathbf{Q}}^{(x)})^{-T} \frac{\partial^2 \mathcal{V}}{\partial \boldsymbol{\gamma}^2} (\hat{\mathbf{Q}}^{(x)})^{-1} \,. \tag{13}$$

Equations 9, 10 and 13 provide the link between the (unknown) depth-domain velocity field and its first and second derivatives to their (known) corresponding ray velocity counterparts, by means of the (unknown) first paraxial ray-tracing matrix $\hat{\mathbf{Q}}^{(x)}$. As seen in the next section, this link will be crucial for the image-ray tracing and time-to-depth conversion algorithm that is proposed here.

Ray-tracing procedure: We suppose that a three-component (ray) coordinate vector, $\boldsymbol{\gamma}$, parameterizes the position and slowness vectors along the ray, $\mathbf{x} = \mathbf{x}(\boldsymbol{\gamma})$ and $\mathbf{p} = \mathbf{p}(\boldsymbol{\gamma})$. The ray is described by setting fixed the two first ray coordinates (γ_1, γ_2) and having the third ray coordinate, γ_3, as the running variable. In our case, the fixed coordinates, $\gamma_1 = x_1^M$ and $\gamma_2 = x_2^M$ specify a trace location in the time-migrated section. The variable coordinate, $\gamma_3 = T$ represents one-way migration time of the image ray that departs from that specified trace location.

Kinematic ray tracing: A basis for kinematic ray tracing in 3D isotropic elastic media can be formulated by the ordinary differential equations (see, e.g., Červený, 2001)

$$\begin{aligned} \frac{d\mathbf{x}}{dT} &= V^2(\mathbf{x})\mathbf{p}, \\ \frac{d\mathbf{p}}{dT} &= -\, V^{-1}(\mathbf{x})\frac{\partial V}{\partial \mathbf{x}}. \end{aligned} \tag{14}$$

Evaluation of the above kinematic ray-tracing equations require the knowledge of the velocity and its first derivatives at points in the depth domain, which we do not immediately have. This information is needed, however, only at the depth-domain points along the image ray that is being traced. More specifically, the velocity and its first derivatives are required only at the points $\mathbf{x} = \mathbf{x}(\boldsymbol{\gamma})$, for varying $\boldsymbol{\gamma}$. In view of the relationships 9 and 10, the kinematic ray-tracing equations can be recast in the form

$$\begin{aligned} \frac{d\mathbf{x}}{dT} &= \mathcal{V}^2(\boldsymbol{\gamma})\mathbf{p}, \\ \frac{d\mathbf{p}}{dT} &= -\, \mathcal{V}^{-1}(\boldsymbol{\gamma})(\hat{\mathbf{Q}}^{(x)})^{-T}\frac{\partial \mathcal{V}}{\partial \boldsymbol{\gamma}}. \end{aligned} \tag{15}$$

In its new form, the ray-tracing system still cannot be solved because of the introduction of the unknown paraxial ray-tracing matrix $\hat{\mathbf{Q}}^{(x)}$. The computation of that matrix can, however, be performed by dynamic ray tracing.

Dynamic ray tracing: We consider a fixed image ray (called the central ray) in a 3D isotropic medium, as well as a family of image rays in its close vicinity (called paraxial rays). To parameterize the family of paraxial rays, we shall use the ray-centered coordinate system, determined by the central ray. As described, e.g., in Červený (2001), this consists of moving a Cartesian (q_I, q_3) coordinate system along the central ray. The time coordinate, $q_3 = T$, specifies the origin, O, on the central ray, of the attached Cartesian system, for which the q_3-axis points in the direction parallel to the slowness vector of the central ray at O. The remaining coordinate axes specify a 2D Cartesian system on the plane normal to the slowness vector of the central ray at O. The two first ray-centered coordinates, q_I, determine a paraxial point, P, on that normal plane.

For each coordinate, q_i, of the ray-centered coordinate system, we associate a corresponding unit basis vector, $\mathbf{e}_i$. These unit vectors constitute the columns of an orthonormal transformation matrix,

$$\hat{\mathbf{H}} = \begin{pmatrix} \mathbf{e}_1 & \mathbf{e}_2 & \mathbf{e}_3 \end{pmatrix} . \tag{16}$$

The matrix $\hat{\mathbf{H}}$ can be computed in any point along the ray if we include within the system of ray differential equations the following equation,

$$\frac{d\mathbf{e}_1}{dT} = -V^2(\mathbf{e}_1 \cdot \frac{d\mathbf{p}}{dT})\mathbf{p} \, , \tag{17}$$

where $d\mathbf{p}/dT$ is given by the second relation in equation 15. Knowing the vector $\mathbf{e}_3 = \mathbf{p}/\|\mathbf{p}\|$ and in addition the vector $\mathbf{e}_1$ resulting from numerical integration including equation 17, the vector $\mathbf{e}_2$ is easily obtained by the cross product

$$\mathbf{e}_2 = \mathbf{e}_3 \times \mathbf{e}_1 \, . \tag{18}$$

In the following, we use the standard formulation of complete dynamic ray tracing in terms of 4×4 matrices in ray-centered coordinates,

$$\frac{d\mathbf{\Pi}}{dT} = \mathbf{S}\mathbf{\Pi} \, . \tag{19}$$

Here, $\mathbf{\Pi}$ is the ray propagator matrix with sub-matrices of size 2×2,

$$\mathbf{\Pi} = \begin{pmatrix} \mathbf{Q}_1^{(q)} & \mathbf{Q}_2^{(q)} \\ \mathbf{P}_1^{(q)} & \mathbf{P}_2^{(q)} \end{pmatrix} , \tag{20}$$

and matrix $\mathbf{S}$ has the definition

$$\mathbf{S} = \begin{pmatrix} \mathbf{0} & V^2\mathbf{I} \\ -V^{-1}\mathbf{V}^{(q)} & \mathbf{0} \end{pmatrix} , \quad \text{where} \quad V_{IJ}^{(q)} = \frac{\partial V}{\partial q_I \partial q_J} \, . \tag{21}$$

By defining a 3×2 sub-matrix of $\hat{\mathbf{H}}$,

$$\bar{\mathbf{H}} = \begin{pmatrix} \mathbf{e}_1 & \mathbf{e}_2 \end{pmatrix} , \tag{22}$$

we relate the 2×2 matrix $\mathbf{V}^{(q)}$ in equation 21 to the 3×3 matrix $\partial^2 V / \partial \mathbf{x}^2$ in equation 13 by

$$\mathbf{V}^{(q)} = \bar{\mathbf{H}}^T \frac{\partial^2 V}{\partial \mathbf{x}^2} \bar{\mathbf{H}} \, . \tag{23}$$

We can now form the sought first paraxial ray tracing matrix $\hat{\mathbf{Q}}^{(x)}$ in depth-domain Cartesian coordinates by the transformation

$$\hat{\mathbf{Q}}^{(x)} = \hat{\mathbf{H}}\hat{\mathbf{Q}}^{(q)} \, , \quad \text{where} \quad \hat{\mathbf{Q}}^{(q)} = \begin{pmatrix} \mathbf{Q}_1^{(q)} & 0 \\ 0 \quad 0 & V \end{pmatrix} . \tag{24}$$

Furthermore, combination of equations 13 and 24 leads to a useful relation for transformation of second derivatives of velocity,

$$\mathbf{V}^{(q)} = (\mathbf{Q}_1^{(q)})^{-T} \frac{\partial^2 \mathcal{V}}{\partial \bar{\boldsymbol{\gamma}}^2} (\mathbf{Q}_1^{(q)})^{-1} \, . \tag{25}$$

where $\bar{\boldsymbol{\gamma}} = (\gamma_1, \gamma_2)^T$. Collecting results, the final set of ordinary differential equations to be integrated along the image ray is specified by equations 15, 17, and 19. An important part of the procedure is on-the-fly transformation of function values, first derivatives, and second derivatives belonging to the time-migration interval velocity field, $\mathcal{V}_{dix}^M(\boldsymbol{\gamma})$, to corresponding quantities in the ray-velocity field along the image ray, $\mathcal{V}(\boldsymbol{\gamma})$. For details concerning such transformations, see Appendix B.

Initial conditions for tracing of the image ray: In order solve the kinematic and dynamic ray-tracing systems, initial conditions have to be provided. These consist of initial values, $\mathbf{x}^0$, $\mathbf{p}^0$, ${\mathbf{e}_1}^0$, and $\mathbf{\Pi}^0$, given for the initial ray coordinate vector $\boldsymbol{\gamma}^0 = (\gamma_1^0, \gamma_2^0, \gamma_3^0)$. Assuming, for simplicity, a planar horizontal datum surface, $x_3 = 0$, for the time-migrated data, we set $\gamma_1^0 = x_1^{M0}$, $\gamma_1^0 = x_2^{M0}$ as the horizontal coordinates of the starting point of the image ray. The given pair (x_1^{M0}, x_2^{M0}), also specifies the trace location in the time-migrated data set that corresponds to the image ray to be constructed. The initial traveltime of the image ray is $\gamma_3^0 = T^0 = 0$.

Since the initial slowness vector of an image ray, $\mathbf{p}^0$, is always perpendicular to the measurement surface, the two horizontal slowness vector components will both be zero, i.e., $p_1^0 = p_2^0 = 0$. The vertical slowness vector component is given by the inverse ray velocity, $p_3^0 = 1/\mathcal{V}_0$, at the trace location (x_1^{M0}, x_2^{M0}) and zero migration time, $t^{M0} = 2T^0 = 0$. Furthermore, one can show (Appendix B) that the factor F in equation 6 has the limit one when the migration time approaches zero; hence, equation 4 yields the initial ray velocity as

$$\mathcal{V}^0 = \mathcal{V}_{dix}^M(\boldsymbol{\gamma}^0) \, . \tag{26}$$

Given the above specifications, the kinematic initial conditions for the image ray read

$$\mathbf{x}^0 = (x_1^{M0}, x_2^{M0}, 0)^T \quad \text{and} \quad \mathbf{p}^0 = (0, 0, \frac{1}{\mathcal{V}^0})^T \ . \tag{27}$$

The initial unit vector ${\mathbf{e}_1}^0$ of the ray-centered coordinate system can be chosen quite freely within the horizontal plane. We shall choose it to be aligned with the profile direction, in other words, ${\mathbf{e}_1}^0 = (\cos\theta, \sin\theta, 0)^T$. Finally, the initial ray propagator matrix, $\mathbf{\Pi}^0$, is the 4×4 identity matrix

$$\mathbf{\Pi}^0 = \begin{pmatrix} \mathbf{I} & \mathbf{0} \\ \mathbf{0} & \mathbf{I} \end{pmatrix} \ . \tag{28}$$

IMPLEMENTATION

A prototype version of the ray-tracing procedure has been implemented in NORSAR's ray-tracing modelling software system (http://www.norsar.com). In the current version of the code, we are able to construct image rays directly from the time-migration interval velocity field, $\mathcal{V}_{dix}^M$. Moreover, horizons belonging to the time-migrated domain may be mapped to the depth domain either by the image-ray method or by stretching along vertical lines. Regularization of the depth-domain velocity field and time-to-depth migration of the full seismic (section/volume) data set based on the image rays have not yet been implemented. An essential part of the implementation is to ensure that the first paraxial ray-tracing matrix $\hat{\mathbf{Q}}^{(x)}$ stays non-singular along the image ray. We do this by monitoring the determinant $\mathrm{det}\hat{\mathbf{Q}}^{(\mathrm{x})}$ as the ray is integrated. If the determinant drops below some predefined limit, currently set to 5% of the initial value, the tracing of the ray is terminated.

EXAMPLES

The theory described above pertains to a three-dimensional subsurface. In this section, we consider, as a first illustration of the method, 2D examples based on a synthetic seismic data set. Since we did not have access to the exact depth-domain macro-velocity model used for generation of the synthetic data, the experiments were, in practice, carried out as blind tests. As a further simplification, we have set the migration velocity spreading factor, F, equal to one. In other words, we have considered that the velocity along the image ray equals the time-migration interval velocity. It is one of our aims in the near future to evaluate the impact of approximate and correct velocity spreading in the obtained images, in 2D and 3D. For our numerical test, we considered the time-migrated section and time-migration velocity field shown in Figure 1. The latter velocity field was converted to a time-migration interval velocity field using equation 5. As we see, this time-migration interval velocity field has drastic variations in the lower central part. The resulting image rays are shown in Figure 2 (top left). Strong focusing occurs in parts of the ray field, which lead to termination of image rays in accordance with the the criterion imposed on the determinant of the matrix $\hat{\mathbf{Q}}^{(x)}$.

In the time-migrated section (Figure 1), three key horizons were picked manually and thereafter mapped to the depth domain using the image rays. Figure 2 (bottom left) shows the resulting depth-domain points (blue). In addition, we performed the time-to-depth mapping along vertical lines. For the upper horizon, the output points (red) from the vertical scaling process are almost identical to the output points from the image-ray mapping. There are, however, significant differences for the dipping parts of the middle and lower horizons.

The variations of the time-migration interval velocity field in Figure 1 were interpreted by the authors as potentially unrealistic. To investigate this further, we did a second experiment based on a modified time-migration interval velocity field (Figure 2, right) for which the drastic variations within the lower central part were replaced by a constant velocity (3.3 km/s). As a result, image rays could be generated without the presence of caustics (Figure 3, top left), which, in turn, made the estimated depth-domain reflectors appear without missing data points (Figure 3, bottom left). As with the more complicated time-migration velocity model, the results of image-ray mapping and vertical scaling are almost identical for the upper reflector, but there are noticeable differences for the flanks of the two lowermost reflectors.

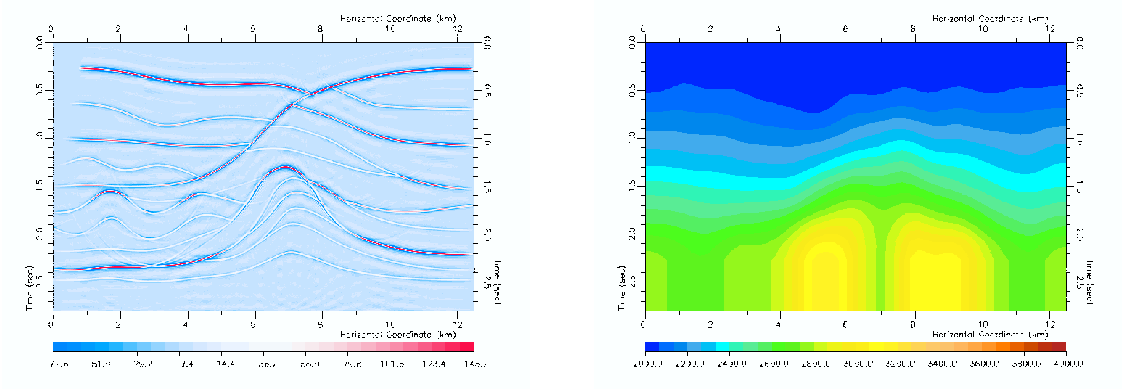

Figure 1: Left: A section in the time-migrated domain. Right: Velocity field $\mathcal{V}^M$ used for migration.

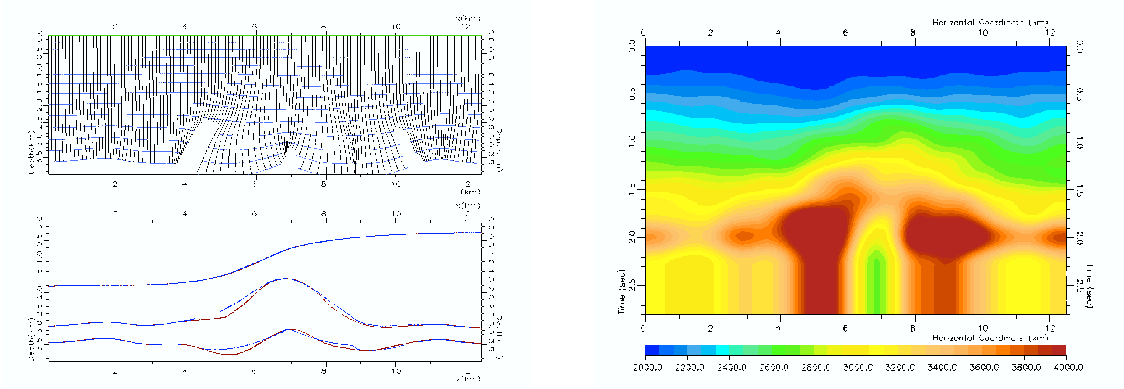

Figure 2: Top left: Image rays (black) and image-ray wavefronts (blue) obtained by applying the ray-tracing procedure to the time-migration interval velocity field in Figure 1. The increment between plotted wavefronts is 0.1s. Bottom left: Depth-domain horizons resulting from time-to-depth mapping along image rays (blue) and vertical lines (red). Right: Time-migration interval velocity field $\mathcal{V}^M_{dix}$, obtained from the migration velocity field in Figure 1 by use of Dix's formula.

DISCUSSION AND CONCLUSIONS

In this paper, we have presented an efficient method to convert selected events or a full time-migrated seismic data set from the time domain to the depth domain. Besides the time-migrated data, all that is needed to initialize the method is the existence of a given migration velocity field, which is transformed into a corresponding field of interval velocities using Dix's algorithm. The resulting time-migration interval velocities are then used to trace image rays in the depth domain and, at the same time, to obtain a depth-domain velocity field along the image rays.

The ray-tracing procedure makes use of ordinary differential equations for position/slowness vectors (kinematic ray-tracing equations) and for the ray propagator matrix expressed in ray-centered coordinates (dynamic ray-tracing equations). The system of differential equations is formulated in such a way that transformations of velocities and their first- and second-order derivatives between coordinate systems for the time-migrated domain and the depth domain are performed on the fly. Thus, as output we get a field of image-ray points and corresponding ray velocities belonging to the depth domain. For each available image ray, one can image an entire seismic trace or map a number of selected events from the time-migrated domain to the depth domain. A final required step is to perform regularization of the estimated ray-velocity field, mapped seismic events, and imaged seismic data with respect to the depth-domain coordinates. The new ray-tracing procedure has been demonstrated for a 2D synthetic data set. The first results indicate the good potential of the method for more complex situations and field data in 2D and 3D. The present

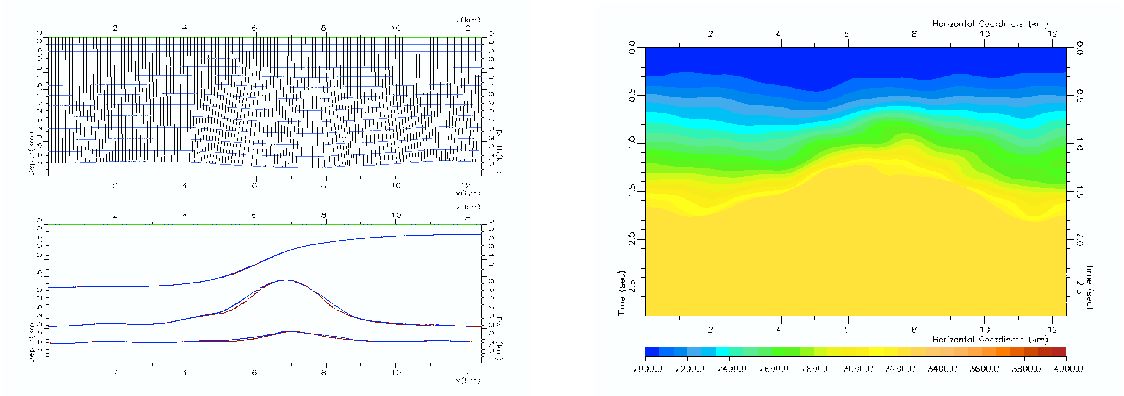

Figure 3: Top left: Image rays (black) and image-ray wavefronts (blue) obtained by the ray-tracing procedure to the edited time-migration interval velocity field in Figure 2. The increment between plotted wavefronts is 0.1s. Bottom left: Depth-domain horizons resulting from time-to-depth mapping along image rays (blue) and along vertical lines (red). Right: An edited version of the time-migration interval velocity field in Figure 2, where velocities in the lower central part have been replaced by a constant value, $\mathcal{V}_{dix}^{M} = 3.3$ km/s.

method is bound to yield best results whenever time migration provides sufficient focusing and also when appropriate time-migration velocities are known. As main advantages, it provides a direct estimation of the depth-domain velocity, with a minimum of user interaction/intervention. The method is very efficient, as compared, for example, to full prestack depth migration and associated estimation of depth-domain velocity parameters. The constraints or limitations of the proposed procedure are the ones basically inherited by the use of the ray method and also Dix's type velocity inversions. For example, for adequate ray-tracing implementation, the time-migration velocity field needs to be "sufficiently smooth" and, moreover, the resolution in the estimation of ray velocity is expected to be poor for deep and/or thin "layers". As an additional condition for effective implementation, care should be taken such that the image-ray field has no triplications and caustics. The 3D approach described in this paper is related, although with some fundamental methodological and implementation differences, to corresponding 2D approaches recently reported by E. Filpo and R. S. Portugal, as well as by M. Cameron, S. Fomel and J. Sethian, which also include applications to field data. In particular, one can observe striking differences between 2D and 3D formulations in the involved complexity of the migration velocity spreading factor and in the closely related dynamic ray tracing procedure. For the 2D situation, it is sufficient to perform dynamic ray tracing only for the plane-wave initial condition, while a proper solution to the 3D problem requires integration also for a point-source solution, which means that the complete ray propagator matrix needs to be computed along the image ray.

ACKNOWLEDGMENTS

E. Iversen acknowledges his colleagues K. Åstebøl and H. Gjøystdal for a fruitful collaboration on the topic of time-to-depth mapping along image rays in the late 1980ies. The work performed at that time was not published as a regular paper, but essential results were, however, presented to the EAEG meeting (Iversen et al., 1987) and in a NORSAR report (Iversen et al., 1988). M. Tygel acknowledges support from the *National Council of Scientific and Technological Development (CNPq)*, Brazil, the *Research Foundation of the State of São Paulo (FAPESP)*, Brazil. This work been also supported by the sponsors of the *Wave Inversion Technology (WIT) Consortium*, Karlsruhe, Germany.

REFERENCES

Cameron, M., Fomel, S., and Sethian, J. (2006). Seismic velocity estimation and time to depth conversion of time-migrated images. In *76th Ann. Internat. Mtg., SEG, Abstracts*, pages 3076–3070.

Filpo, E. and Portugal, R. (2006). Time-to-depth conversion by auto propagation of image wavefronts. *Submitted to Geohys. Prosp.*

Fomel, S. (2003). Time migration velocity analysis by velocity continuation. *Geophysics*, 68:1662–1672.

Hale, D. (1984). Dip-moveout by Fourier transform. *Geophysics*, 49(06):741–757.

Hubral, P. (1977). Time migration - some ray theoretical aspects. *Geophys. Prosp.*, 25(04):738–745.

Hubral, P. and Krey, T. (1980). Interval Velocities from Seismic Reflection Time Measurements. Soc. of Expl. Geophys.

Hubral, P., Schleicher, J., and Tygel, M. (1992). Three-dimensional paraxial ray properties: – basic relations. *Journal of Seismic Exploration*, 1:347–279.

Iversen, E. (2006). Amplitude, Fresnel zone, and NMO velocity for PP and SS normal-incidence reflections. *Geophysics*, 71:W1–W14.

Iversen, E., Åstebøl, K., and Gjøystdal, H. (1987). Time-to-depth conversion of 3D seismic interpretation data by use of 'dynamic image rays'. In *49th Ann. Internat. Mtg., Eur. Ass. of Expl. Geophys., Abstracts*, page 16.

Iversen, E., Åstebøl, K., and Gjøystdal, H. (1988). 3D time-to-depth conversion of interpreted time-migrated horizons by use of the paraxial image ray method. *Research report, NORSAR, Norway*.

Tygel, M., Schleicher, J., and Hubral, P. (1996). A unified approach to 3-D seismic reflection imaging, part II: Theory. *Geophysics*, 61(03):759–775.

Červený, V. (2001). *Seismic Ray Theory*. Cambridge University Press.

Yilmaz, O. (2000). *Seismic Data Analysis*. Soc. of Expl. Geophys.

APPENDIX A

APPENDIX A: VELOCITY SPREADING FACTOR FOR THE IMAGE RAY

In this appendix, we derive equation 6 for the velocity spreading factor, F. Since all matrices considered here belong to ray-centered coordinates, we have skipped the superscript (q) for clarity. Our starting point is an equation relating the (azimuth-dependent) migration velocity, $\mathcal{V}^M$, to the 2×2 matrix, $\mathbf{M}_2^{\uparrow}$, of second derivatives of one-way, upward, traveltime

$$T(\mathcal{V}^M)^2 = \frac{1}{\bar{\mathbf{u}}^T \mathbf{M}_2^{\uparrow} \bar{\mathbf{u}}} \, . \tag{A-1}$$

In the above equation, T, is the one-way, downward, migrated time and $\bar{\mathbf{u}}$ is the direction vector along the profile used to obtain the migration velocity, $\mathcal{V}^M$. Substituting equation A-1 into the Dix velocity equation 5, we obtain the important relation

$$(\mathcal{V}_{dix}^M)^2 = -\frac{1}{(\bar{\mathbf{u}}^T \mathbf{M}_2^{\uparrow} \bar{\mathbf{u}})^2} \left[\bar{\mathbf{u}}^T \frac{d\mathbf{M}_2^{\uparrow}}{dT} \bar{\mathbf{u}} \right] \, . \tag{A-2}$$

It is our aim to express the matrices $\mathbf{M}_2^{\uparrow}$ and $d\mathbf{M}_2^{\uparrow}/dT$ in terms of downgoing matrices that can be obtained in the image-ray tracing that we have in mind. Following standard theory of paraxial ray-tracing matrices (see, e.g., Červený, 2001), the matrix $\mathbf{M}_2^{\uparrow}$ can be expressed in terms of the paraxial ray-tracing matrices $\mathbf{Q}_2^{\uparrow}$ and $\mathbf{P}_2^{\uparrow}$ of size 2×2,

$$\mathbf{M}_2^{\uparrow} = \mathbf{P}_2^{\uparrow} \mathbf{Q}_2^{\uparrow^{-1}} \, . \tag{A-3}$$

Furthermore, following Iversen (2006), the upward propagation matrices, $\mathbf{Q}_2^{\uparrow}$ and $\mathbf{P}_2^{\uparrow}$, can be expressed in term of downward propagation counterparts as

$$\mathbf{Q}_2^{\uparrow} = \mathbf{I}^* {\mathbf{Q}_2^{\downarrow}}^T \mathbf{I}^* \quad \text{and} \quad \mathbf{P}_2^{\uparrow} = \mathbf{I}^* {\mathbf{Q}_1^{\downarrow}}^T \mathbf{I}^* \,, \tag{A-4}$$

where $\mathbf{I}^*$ is the matrix previously given by equation 7. Substituting into equation A-3 and applying the derivative with respect to T yields

$$\mathbf{M}_2^{\uparrow} = \mathbf{I}^* {\mathbf{Q}_1^{\downarrow}}^T {\mathbf{Q}_2^{\downarrow}}^{-T} \mathbf{I}^* \quad \text{and} \quad \frac{d\mathbf{M}_2^{\uparrow}}{dT} = \mathbf{I}^* \frac{d}{dT}[{\mathbf{Q}_1^{\downarrow}}^T {\mathbf{Q}_2^{\downarrow}}^{-T}]\mathbf{I}^* \,. \tag{A-5}$$

We also observe that, for an isotropic medium, the differential equation for paraxial ray-tracing matrix $\mathbf{Q}_I^{\downarrow}$, for $I = 1, 2$, is

$$\frac{d\mathbf{Q}_I^{\downarrow}}{dT} = V^2 \mathbf{P}_I^{\downarrow} \quad \text{and also} \quad \frac{d{\mathbf{Q}_I^{\downarrow}}^{-1}}{dT} = -\, V^2 {\mathbf{Q}_I^{\downarrow}}^{-1} \mathbf{P}_I^{\downarrow} {\mathbf{Q}_I^{\downarrow}}^{-1} \,. \tag{A-6}$$

The rightmost equation was obtained under the application of the generic formula

$$\frac{d\mathbf{A}^{-1}}{dT} = -\, \mathbf{A}^{-1} \frac{d\mathbf{A}}{dT} \mathbf{A}^{-1} \,, \tag{A-7}$$

which results from differentiating both sides of the identity $\mathbf{A}^{-1}\mathbf{A} = \mathbf{I}$, followed by the application of the leftmost equation A-6. Using the chain rule and also taking into account equations A-6, we get

$$\frac{d}{dT}[{\mathbf{Q}_1^{\downarrow}}^T {\mathbf{Q}_2^{\downarrow}}^{-T}] = \mathcal{V}^2 \left\{ \left[{\mathbf{P}_1^{\downarrow}}^T - {\mathbf{Q}_1^{\downarrow}}^{-T} {\mathbf{Q}_2^{\downarrow}}^{-T} {\mathbf{P}_2^{\downarrow}}^T \right] {\mathbf{Q}_2^{\downarrow}}^{-T} \right\} \,, \tag{A-8}$$

where we observed that, along the image ray, $V(\mathbf{x}) = \mathcal{V}(\boldsymbol{\gamma})$. Taking into account the identities

$${\mathbf{Q}_2^{\downarrow}}^{-T} {\mathbf{P}_2^{\downarrow}}^T = \mathbf{P}_2^{\downarrow} {\mathbf{Q}_2^{\downarrow}}^{-1} \quad \text{and} \quad {\mathbf{Q}_1^{\downarrow}}^T \mathbf{P}_2^{\downarrow} - {\mathbf{P}_1^{\downarrow}}^T \mathbf{Q}_2^{\downarrow} = \mathbf{I} \,, \tag{A-9}$$

which are properties of the ray propagator matrix (Červený, 2001), we find that

$$\frac{d}{dT}[{\mathbf{Q}_1^{\downarrow}}^T {\mathbf{Q}_2^{\downarrow}}^{-T}] = \mathcal{V}^2 \left\{ \left[{\mathbf{P}_1^{\downarrow}}^T \mathbf{Q}_2^{\downarrow} - {\mathbf{Q}_1^{\downarrow}}^{-T} {\mathbf{P}_2^{\downarrow}}^T \right] {\mathbf{Q}_2^{\downarrow}}^{-1} {\mathbf{Q}_2^{\downarrow}}^{-T} \right\} = -\, \mathcal{V}^2 {\mathbf{Q}_2^{\downarrow}}^{-1} {\mathbf{Q}_2^{\downarrow}}^{-T} \,. \tag{A-10}$$

Substitution into equation A-5 and further into the Dix velocity formula A-2 yields

$$(\mathcal{V}_{dix}^M)^2 = -\frac{1}{(\bar{\mathbf{u}}^T \mathbf{M}_2^{\uparrow} \bar{\mathbf{u}})^2} \left[\bar{\mathbf{u}}^T \frac{d\mathbf{M}_2^{\uparrow}}{dT} \bar{\mathbf{u}} \right] = \mathcal{V}^2 \left\{ \frac{\bar{\mathbf{u}}^T \mathbf{I}^* {\mathbf{Q}_2^{\downarrow}}^{-1} {\mathbf{Q}_2^{\downarrow}}^{-T} \mathbf{I}^* \bar{\mathbf{u}}}{(\bar{\mathbf{u}}^T \mathbf{I}^* {\mathbf{Q}_1^{\downarrow}}^T {\mathbf{Q}_2^{\downarrow}}^{-T} \mathbf{I}^* \bar{\mathbf{u}})^2} \right\} \,. \tag{A-11}$$

We conclude that

$$F^2 = \frac{\mathcal{V}^2}{(\mathcal{V}_{dix}^M)^2} = \frac{(\bar{\mathbf{u}}^T \mathbf{I}^* {\mathbf{Q}_1^{\downarrow}}^T {\mathbf{Q}_2^{\downarrow}}^{-T} \mathbf{I}^* \bar{\mathbf{u}})^2}{\bar{\mathbf{u}}^T \mathbf{I}^* {\mathbf{Q}_2^{\downarrow}}^{-1} {\mathbf{Q}_2^{\downarrow}}^{-T} \mathbf{I}^* \bar{\mathbf{u}}} \,, \tag{A-12}$$

which is equivalent to equation 6 given in the main text.

APPENDIX B: COMPUTATION OF VELOCITY DERIVATIVES

In this appendix, we describe an approach for computation of the first and second derivatives, $d\mathcal{V}/d\boldsymbol{\gamma}$ and $d^2\mathcal{V}/d\boldsymbol{\gamma}^2$ at each ray coordinate, $\boldsymbol{\gamma}$, that are required for our image-ray tracing scheme. Observe that we write here the paraxial ray-tracing matrices without the superscript (q). Twice differentiation of equation 4 yields

$$\frac{\partial \mathcal{V}}{\partial \gamma_i} = \frac{\partial \mathcal{V}_{dix}^M}{\partial \gamma_i} F + \mathcal{V}_{dix}^M \frac{\partial F}{\partial \gamma_i} \tag{B-1}$$

and

$$\frac{\partial^2 \mathcal{V}}{\partial \gamma_i \partial \gamma_j} = \frac{\partial^2 \mathcal{V}_{dix}^M}{\partial \gamma_i \partial \gamma_j} F + \left[\frac{\partial \mathcal{V}_{dix}^M}{\partial \gamma_i} \frac{\partial F}{\partial \gamma_j} + \frac{\partial \mathcal{V}_{dix}^M}{\partial \gamma_j} \frac{\partial F}{\partial \gamma_i} \right] + \mathcal{V}_{dix}^M \frac{\partial^2 F}{\partial \gamma_i \partial \gamma_j} \,. \tag{B-2}$$

Since $\mathcal{V}_{dix}^{M}$ and its derivatives are known, our problem reduces to find the derivatives of the factor F, which has the form

$$F = \frac{A}{B^{1/2}} \,, \tag{B-3}$$

where

$$A = \bar{\mathbf{u}}^T \mathbf{I}^* \mathbf{Q}_1^T \mathbf{Q}_2^{-T} \mathbf{I}^* \bar{\mathbf{u}} \,, \qquad B = \bar{\mathbf{u}}^T \mathbf{I}^* \mathbf{Q}_2^{-1} \mathbf{Q}_2^{-T} \mathbf{I}^* \bar{\mathbf{u}} \,. \tag{B-4}$$

Using equation B-3, we find the following relations between first- and second-order derivatives of the factors F, A, and B,

$$\frac{\partial F}{\partial \gamma_i} = \frac{1}{2B^{3/2}} (2B \frac{\partial A}{\partial \gamma_i} - A \frac{\partial B}{\partial \gamma_i}) \,, \tag{B-5}$$

$$\frac{\partial^2 F}{\partial \gamma_i \partial \gamma_j} = \frac{1}{2B^{5/2}} \left[(A \frac{\partial B}{\partial \gamma_i} - B \frac{\partial A}{\partial \gamma_i}) \frac{\partial B}{\partial \gamma_j} + B(2B \frac{\partial^2 A}{\partial \gamma_i \partial \gamma_j} - A \frac{\partial^2 B}{\partial \gamma_i \partial \gamma_j}) \right] \,. \tag{B-6}$$

Here, the derivatives of A and B can be obtained by straightforward differentiation of equation B-4. Note, however, that since the factors A, B, and thus also F, depend on all three ray coordinates γ_1, γ_2, and γ_3, an exact solution for the factor F cannot, in general, be obtained by numerical integration along a single ray subjected to the standard second-order traveltime approximation.

Based on the above, we propose three alternative approximations for the factor F and its derivatives which all can be incorporated in a time-to-depth conversion strategy where computations along one ray are independent of those along neighboring rays. The first, simplest, alternative is to assume that the factor F is one along the whole image ray. As a second alternative, we assume that the factor F is only locally constant, which means that all partial derivatives of F will be ignored in the computations. Finally, as the the third approximation, we assume that F is a function of the traveltime, $\gamma_3 = T$, only. In this case, only the derivatives of F with respect to T in equations B-5-B-6 survive, and equations B-1-B-2 can therefore be restated as

$$\frac{\partial \mathcal{V}}{\partial \gamma_I} = \frac{\partial \mathcal{V}_{dix}^{M}}{\partial \gamma_I} \, F \,, \qquad \frac{\partial \mathcal{V}}{\partial T} = \frac{\partial \mathcal{V}_{dix}^{M}}{\partial T} \, F + \mathcal{V}_{dix}^{M} \frac{\partial F}{\partial T} \,, \tag{B-7}$$

$$\frac{\partial^2 \mathcal{V}}{\partial \gamma_I \partial \gamma_J} = \frac{\partial^2 \mathcal{V}_{dix}^{M}}{\partial \gamma_I \partial \gamma_J} \, F \,, \qquad \frac{\partial^2 \mathcal{V}}{\partial T^2} = \frac{\partial^2 \mathcal{V}_{dix}^{M}}{\partial T^2} \, F + 2 \frac{\partial \mathcal{V}_{dix}^{M}}{\partial T} \, \frac{\partial F}{\partial T} + \mathcal{V}_{dix}^{M} \, \frac{\partial^2 F}{\partial T^2} \,. \tag{B-8}$$

One can show, however, that our integration procedure does not rely on the second derivatives $\partial^2 \mathcal{V} / \partial T^2$, which means that calculation of the second derivative $\partial^2 F / \partial T^2$, as specified by equation B-6, is not required. Considering equation B-5, the first derivative of F with respect to time is

$$\frac{\partial F}{\partial T} = \frac{1}{2B^{3/2}} (2B \frac{\partial A}{\partial T} - A \frac{\partial B}{\partial T}) \,. \tag{B-9}$$

Differentiation of the two relations in equation B-4 yields

$$\frac{\partial A}{\partial T} = \bar{\mathbf{u}}^T \mathbf{I}^* \left(\frac{\partial \mathbf{Q}_1^T}{\partial T} \mathbf{Q}_2^{-T} + \mathbf{Q}_1^T \frac{\partial \mathbf{Q}_2^{-T}}{\partial T} \right) \mathbf{I}^* \bar{\mathbf{u}} \,, \quad \frac{\partial B}{\partial T} = 2 \bar{\mathbf{u}}^T \mathbf{I}^* \left(\frac{\partial \mathbf{Q}_2^{-1}}{\partial T} \mathbf{Q}_2^{-T} \right) \mathbf{I}^* \bar{\mathbf{u}} \,, \tag{B-10}$$

where the derivative of the inverse matrix is given by

$$\frac{\partial \mathbf{Q}_2^{-1}}{\partial T} = -\mathbf{Q}_2^{-1} \frac{\partial \mathbf{Q}_2}{\partial T} \mathbf{Q}_2^{-1} \,. \tag{B-11}$$

For calculation of derivatives of matrices $\mathbf{Q}_I$ with respect to traveltime, see equation 19.

It must be noted that the above formulas for factor F and its derivatives cannot be used for zero migration time, for which $B = 0$. We find, however, that a second-order approximation for the factor F in the vicinity of $T = 0$ is given by

$$F = 1 - \frac{1}{2} \mathcal{V} T^2 \bar{\mathbf{u}}^T \mathbf{I}^* \frac{\partial^2 \mathcal{V}}{\partial \bar{\gamma}^2} \mathbf{I}^* \bar{\mathbf{u}} \,, \tag{B-12}$$

which yields, at $T = 0$,

$$F = 1 \,, \qquad \frac{\partial F}{\partial T} = 0 \,. \tag{B-13}$$

In the 2D situation, we have

$$F = Q_1 \ , \qquad \frac{\partial F}{\partial T} = \frac{\partial Q_1}{\partial T} = \mathcal{V}^2 P_1 \ , \tag{B-14}$$

which is reduced to equation B-13 in the limit of zero time ($Q_1 = 1$; $P_1 = 0$).